Journal of
Environmental & Analytical Toxicology

Sheng et al., J Environ Anal Toxicol 2016, 6:3
DOI: 10.4172/2161-0525.1000372

Research Article Open Access

Preparation and Photocatalytic Activity of Ag-Modified SnO_2@TiO_2 Core-Shell Composites

Jianguo Sheng*, Hui Xu and Cong Tang

Institute of Environmental and Chemical Engineering, Jiangsu University of Science and Technology, Zhenjiang, Jiangsu, PR China

Abstract

Photocatalytic degradation is an important method to mediate organic pollution in the environment. This article reports Ag-modified SnO_2@TiO_2 core-shell composite photocatalysts prepared via a hydrothermal method. The composite materials were characterized by X-ray diffraction, transmission electron microscopy, energy dispersive X-ray spectroscopy, thermogravimetry, X-ray photoelectron spectrometry, and UV-vis diffuse reflectance spectroscopy. The Ag modification and core structure in the composite enhanced the photocatalytic activity and stability of TiO_2 for Rhodamine B degradation under visible light irradiation. The composite modified in 0.15 M $AgNO_3$ showed an optimal level of photocatalytic activity, as it degraded 99.14% of Rhodamine B in 60 min while pure TiO_2 only degraded 45.7% during the same time.

Keywords: Core-shell composites; Hydrothermal method; Photocatalytic activity

Abbreviations: PT: Pure TiO_2; AgT: Ag-modified TiO_2; ST: SnO_2@TiO_2; AgST: Ag-modified SnO_2@TiO_2; AgST-M: Ag-modified SnO_2@TiO_2 prepared with M mol L^{-1} $AgNO_3$

Introduction

Recently, titanium dioxide (TiO_2) has attracted great interest for the degradation of pollutants [1-3], such as most organic compounds and inorganic ions [4,5]. However, the photocatalytic performance of TiO_2 is greatly restricted by its wide band gap (3.2 eV) and high electron-hole recombination rate. Proposed solutions to these problems include doping with metallic or nonmetallic ions [6,7], dye photosensitization on the TiO_2 surface [8], deposition of noble metals [9,10], and semiconductor modification [11].

Modifying TiO_2 with semiconductors such as SnO_2 has proven to be an effective way to improve the photocatalytic activity, by using the transport and separation of photo produced carriers between two semiconductors with different energy gaps. Separately, Ag or other noble metals deposited on the surface of TiO_2 form a short-circuit battery with TiO_2, which leads to effective separation of the photogenerated electrons/holes and a lower potential in the reduction reaction, thus greatly improving the photocatalytic activity.

In this paper, Ag-modified SnO_2@TiO_2 core-shell composites were fabricated in two steps: first the synthesis of SnO_2@TiO_2 composite using a hydrothermal method, and then surface modification of the composite with Ag. The Ag-modified SnO_2@TiO_2 core-shell composites demonstrated excellent photocatalytic activity and cycle stability under visible light.

Materials and Methods

Preparation of Ag-modified SnO_2@TiO_2 core-shell composites

Preparation of SnO_2: $SnCl_4 \cdot 5H_2O$ and polyethylene glycol (PEG) were added into deionized water and magnetically stirred. When $SnCl_4 \cdot 5H_2O$ was completely dissolved, excessive ammonia was added dropwise into the solution and stirred well. After filtration, the precipitate was washed with absolute alcohol, and calcined at 400°C for 2 h to obtain the SnO_2 powder.

Preparation of SnO_2@TiO_2 core-shell composites: Tetrabutyl titanate, acetic acid, and anhydrous alcohol were mixed together, and then alcohol-water solution was slowly added to the mixture and stirred for 30 min. SnO_2 was then added, followed by another 30 min of stirring. The obtained solution was transferred to a 100-mL Teflon-lined autoclave and kept in an oven at 150°C for 4 h. After cooling to room temperature, the precipitate was collected by centrifugation (6000 rpm, 20 min), washed with anhydrous alcohol, and then dried at 60°C overnight. The obtained SnO_2@TiO_2 sample is designated as ST.

Preparation of Ag-modified SnO_2@TiO_2 core-shell composites: The ST composite was added to $AgNO_3$ solutions of given concentrations and irradiated under a 500 W mercury lamp. The solids were collected by centrifugation and dried at 60°C overnight to obtain Ag-modified SnO_2@TiO_2 core-shell composites. These samples are designated as AgST-M, where M is the molar concentration of $AgNO_3$ solution used. For comparison, pure TiO_2 and Ag-modified TiO_2 were synthesized separately, and designated as PT and AgT, respectively.

Characterization of the photocatalysts

The chemical composition of the photocatalyst samples was analyzed by energy dispersive X-ray spectroscopy (EDX, INCA). Transmission electron microscopy (TEM, JEM-2100, JEOL) was used for morphology characterization. The crystalline structures of the samples were determined by X-ray diffraction (XRD, XRD-6000, Japan Shimadzu) using Cu Ka radiation (λ=0.154 nm) at 40 kV, 250 mA at room temperature. An X-ray photoelectron spectrometer (XPS, Thermo ESCALAB 250, Waltham, MA, USA) was used to analyze the elemental composition and valence states. UV-vis diffuse reflectance

***Corresponding author:** Jianguo Sheng, Institute of Environmental and Chemical Engineering, Jiangsu University of Science and Technology, Zhenjiang, Jiangsu, PR China, Tel: 8651184401002; E-mail: sjg6418@sina.com

Received March 16, 2016; **Accepted** May 10, 2016; **Published** May 15, 2016

Citation: Sheng J, Xu H, Tang C (2016) Preparation and Photocatalytic Activity of Ag-Modified SnO_2@TiO_2 Core-Shell Composites. J Environ Anal Toxicol 6: 372. doi:10.4172/2161-0525.1000372

spectra (DRS) of the samples were recorded in the range of 200–800 nm using a Shimadzu UV240 spectrophotometer (Kyoto, Japan) equipped with an integrating sphere, and $BaSO_4$ was used as the reference. Thermogravimetry and differential thermal analysis (TG-DTA) were performed by a Pyris Diamond 851e analyzer (PerkinElmer) at a heating rate of 200°C min^{-1} under N_2 environment, with a flow rate of 50 mL min^{-1}.

Photocatalytic activity

The photocatalytic activities of the samples were evaluated by the degradation of Rhodamine B in a 500-mL jacketed beaker, a 500 W mercury lamp was selected as the visible light source. In a typical experiment, 0.05 g of the photocatalyst sample was dispersed in the Rhodamine B solution (40 mL, 5 mg L^{-1}). The solution was then maintained in the dark for 30 min prior to irradiation, in order to reach the adsorption-desorption equilibrium. During irradiation, 4 mL of the sample solution was taken out every 10 min and the Rhodamine B concentration was measured by UV-vis spectroscopy. The degradation rate of Rhodamine B can be calculated via the formula:

$$\eta = (1 - A_i / A_0) \times 100\%$$

where A_0 is the initial absorbance of the solution, and A_i is the absorbance after different reaction times.

Results and Discussion

Phase structure and morphology characterization

The XRD spectra of Ag-modified SnO_2@TiO_2 and other samples were shown in Figure 1. The diffraction patterns of ST and AgST displayed the anatase peak of TiO_2 at 2θ = 25.3°. However, we could not confirm the anatase phase since only one peak was detected, probably due to the low amount of TiO_2 in the particles. Similarly, no Ag peaks were detected in the patterns of AgT and AgST, likely due to the low amount of Ag [12-14].

Figure 2 showed three typical TEM images of AgST-0.15. The as-prepared sample consisted of many decentralized nanoparticles of uniform size (30–50 nm in diameter). The core-shell nanostructures could be observed in Figure 2(c), as the surface of the SnO_2 nanoparticles was coated with a layer of TiO_2.

Thermogravimetric analysis

TG-DTA curves of the AgST-0.15 nanoparticles were exhibited in Figure 3. The results showed that the nanoparticles underwent a multistep decomposition process in the temperature range of 25–800°C. The endothermic peak in the range of 25–90°C was related to the desorption of physically adsorbed free water and residual ethanol, which together accounted for 8% of the weight loss. The sharp exothermic peak in the temperature range of 200–300°C (about 5% weight loss) was due to the combustion of organics on the surface of the sample. In the temperature range of 300–400°C, there was another exothermic peak owing to further carbonization of organics and the removal of constitution water. These results indicated that the as-prepared Ag-modified SnO_2@TiO_2 core-shell composite exhibited high thermal stability.

Elemental analysis

XPS analysis: AgST-0.15 was further analyzed by XPS to determine the main elements on the TiO_2 surface and their chemical states. The survey spectrum was shown in Figure 4(a). The binding energies obtained in the analysis were corrected for specimen charging by C ls

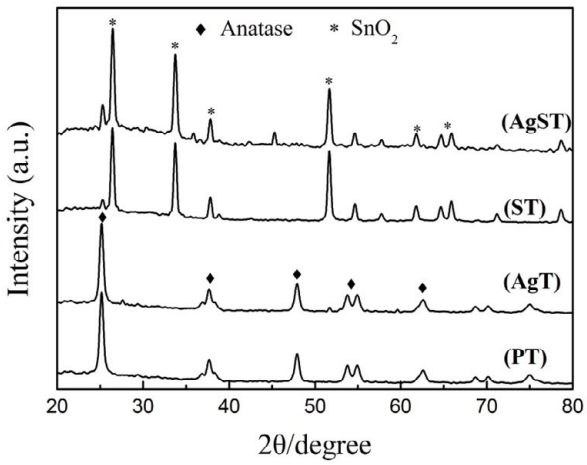

Figure 1: XRD patterns of different samples.

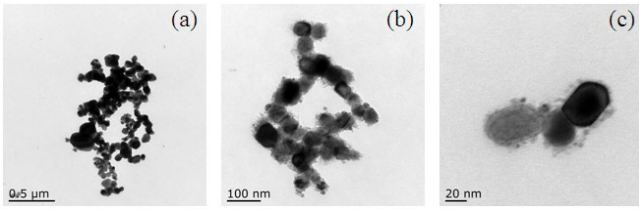

Figure 2: TEM images of AgST-0.15 composite at different levels of magnification.

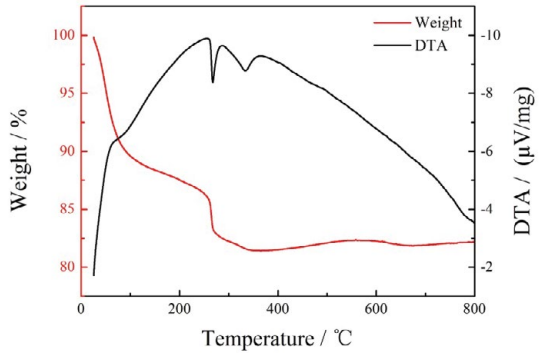

Figure 3: TG-DTA curves of the AgST-0.15 composite.

(284.8 eV) [15]. The results indicated the presence of five elements: C, Ti, O, Sn, and Ag. In Figure 4(b), the two Sn 3d peaks centered at 495.2 and 486.9 eV were assigned as Sn $3d_{3/2}$ and Sn $3d_{5/2}$, respectively. The binding energy of Sn $3d_{5/2}$ (486.9 eV) matched the typical values for SnO_2 [16,17], indicating that the Sn^{4+} dopant was incorporated into TiO_2 to form SnO_2. In the spectrum of Ag 3d (Figure 4(c)), the binding energies of 368.2 and 374.2 eV were respectively attributed to Ag $3d_{5/2}$ and Ag $3d_{3/2}$. The 6.0 eV splitting within the Ag 3d doublet indicated the formation of metallic Ag on the surface of TiO_2 [18,19]. The Ag content of AgST-0.15 estimated from XPS was 3.76%. The atomic ratio of O/Ti

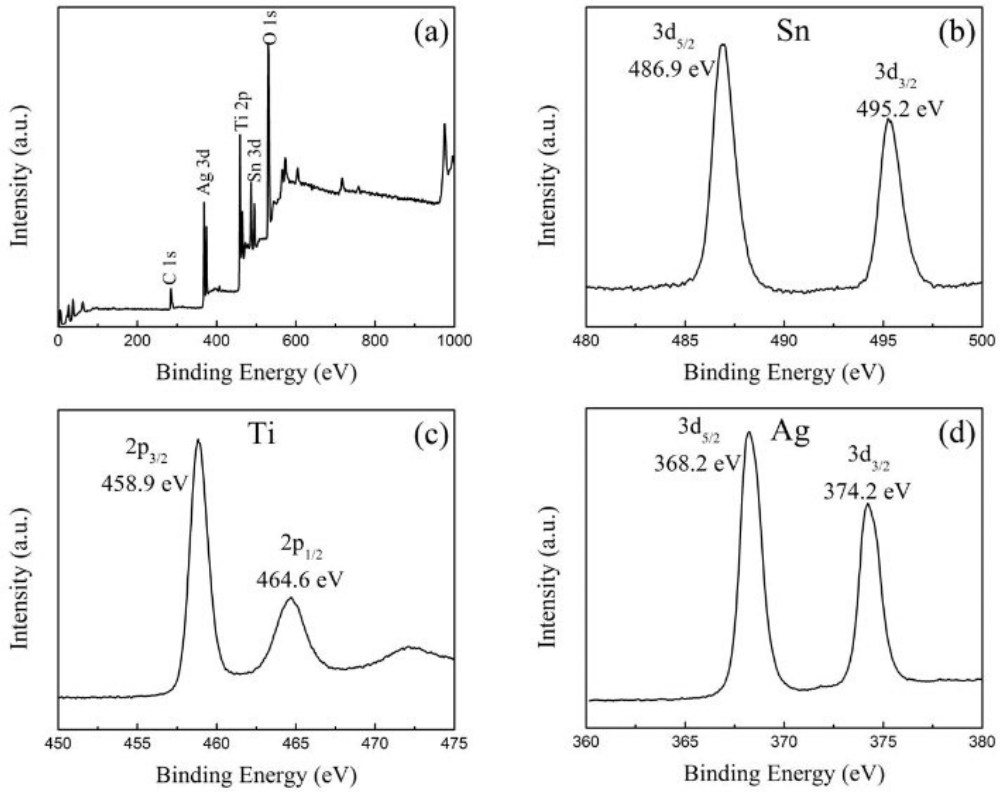

Figure 4: XPS spectra of AgST-0.15: (a) survey spectra, (b) Sn 3d, (c) Ti 2p, and (d) Ag 3d.

determined from XPS was 2.82:1, suggesting the existence of oxygen vacancies on the surface of TiO_2.

EDX analysis: The AgST-0.15 sample was analyzed by EDX in order to determine its composition (Figure 5). Elemental analysis results (Table 1) showed only Ti, O, Ag and Sn with no detectable impurities, which are in agreement with the XPS results.

Photoelectrochemical performance

UV-Vis DRS analysis: The activity of a photocatalyst mainly depends on the width of its band gap, and the recombination rate of electron-hole pairs. From the UV-vis DRS results in Figure 6, the band gaps for PT, AgT, ST, and AgST-0.15 were estimated to be 3.17, 3.06, 3.02, and 2.85 eV, respectively. Compared to PT, both AT and ST exhibited enhanced absorption extending towards the visible region. AgST-0.15 exhibited significant absorption in both UV and visible regions, revealing the synergistic effects of SnO_2 addition and Ag modification in narrowing the band gap of TiO_2. This obtained result could be ascribed to the following mechanisms: (1) electron transfer from TiO_2 surface to SnO_2, which reduced the electron density on the TiO_2 surface, as well as the rate of recombination of photogenerated holes and electrons [20,21], (2) Ag with its high electrical conductivity can transfer electrons during the photocatalytic reaction, thereby dispersing the electrons and photogenerated holes [22].

Photocatalytic activity in Rhodamine B degradation: The photocatalytic activities of the samples were evaluated by the degradation of Rhodamine B under visible light irradiation, with the results shown in Figure 7. The degradation rates were relative to the

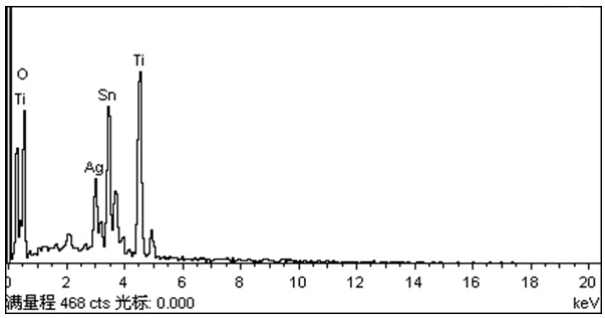

Figure 5: EDX patterns of AgST-0.15

Rhodamine B concentration at adsorption equilibrium (after 30 min in the dark). Compared with PT, all modified TiO_2 samples showed improved photocatalytic performance, especially the Ag-modified SnO_2@TiO_2 core-shell composites, which remarkably accelerated the photodegradation. Importantly, the photocatalytic efficiency initially increased with the concentration of $AgNO_3$ used for treatment, from 0 to 0.1 and then 0.15 M. Afterwards, the efficiency decreased with $AgNO_3$ concentration up to 0.3 M. The AgST-0.15 sample exhibited the best catalytic efficiency, degrading 99.14% of Rhodamine B in 60 min while PT only degraded 45.7% during the same time period.

Photochemical stability of the catalysts

Figure 8 compared the cycle stability of AgST-0.15, the most

Element	Weight percent (%)	Atomic percent (%)
O K	50.32	82.85
Ti K	18.10	9.95
Ag L	8.71	2.13
Sn L	22.87	5.08
Total	100.00	100.01

Table 1: The elemental composition of AgST-0.15.

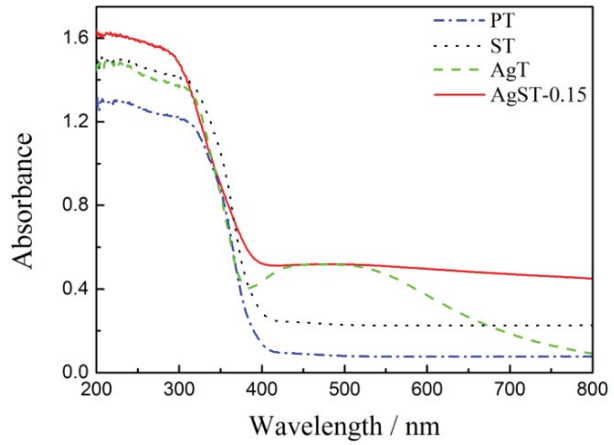

Figure 6: UV-vis diffuse reflectance spectra of different photocatalyst samples.

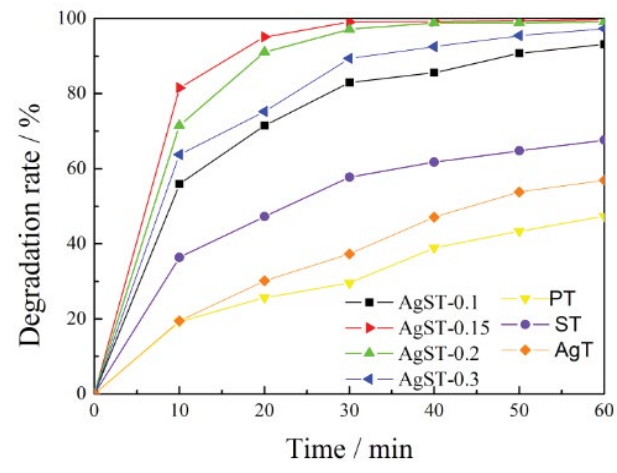

Figure 7: The degradation curves of Rhodamine B under visible light irradiation with different photocatalysts.

effective Ag-modified catalyst, and unmodified PT. The activity of PT was approximately halved, from 45.7% to 23.63%, after 4 catalytic cycles of 60 min each. In contrast, AgST-0.15 maintained a high level of catalytic activity after the same number of cycles.

Conclusion

Ag-modified SnO_2@TiO_2 core-shell composites were successfully prepared by a hydrothermal method. Compared with pure TiO_2, the composite sample had significantly higher photocatalytic activity in visible light due to the synergistic effect of Ag modification and SnO_2

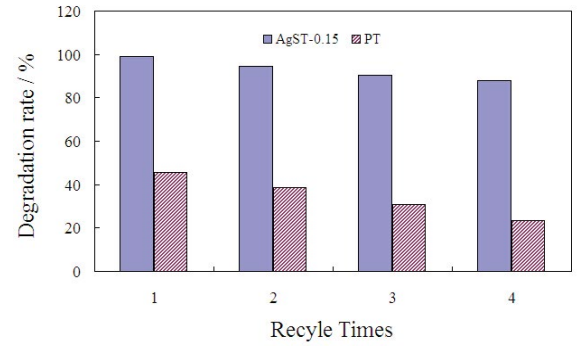

Figure 8: Photochemical stability of AgST-0.15 and PT. The degradation rate is based on 60 min of reaction time.

addition. The photocatalytic activity of Ag-modified SnO_2@TiO_2 core-shell composites was better than the published results for TiO_2-SnO_2 [23]. Since Ag has good electrical conductivity, it can facilitate the electron transfer during the photocatalytic reaction, and disperse the electrons and photogenerated holes. However, excess Ag may cover the surface of TiO_2, thereby reducing the photocatalytic rate. Hence, there was an optimal Ag content for photocatalysis, beyond which the efficiency would decrease. The sample modified with 0.15 M $AgNO_3$ possessed the best photocatalytic performance, as well as cycle stability.

References

1. Fujishima A, Rao TN, Tyrk DA (2000) Titanium dioxide photocatalysis. J Photochem Photobio C Photochem Rev 1: 1-21.
2. Carp O, Huisman CL, Reller A (2004) Photoinduced reactivity of titanium dioxide. Prog Solid State Chem 32: 33-177.
3. Zhao J, Yang XD (2003) Photocatalytic oxidation for indoor air purification. Build Environ 38: 645-654.
4. Ohko Y, Saitoh S, Tatsuma T, Fujishima A (2001) Photoelectrochemical anticorrosion and self-cleaning effects of a TiO_2 coating for type 304 stainless steel. J Electrochem Soc 148: 24-28.
5. Subasri R, Shinohara T (2004) Application of the photoeffect in TiO_2 for cathodic protection of copper. Electrochem 72: 880-884.
6. Yuan JN, Tsujikawa S (1995) Characterization of sol-gel-derived TiO_2 coatings and their photoeffects on copper substrates. J Electrochem Soc 142: 3444-3450.
7. Song LZ, Zhao J, Wang XL (2005) Modification and anticorrosion property of carbon steel with TiO_2 film. J Iron Steel Res Int 12: 37-41.
8. Xie K, Sun L, Wang C, Lai Y, Wang M, et al. (2010) Photo electrocatalytic properties of Ag nanoparticles loaded TiO2 nanotube arrays prepared by pulse current deposition. Electrochim Acta 55: 7211-7218.
9. Li SN, Fu JJ (2013) Improvement in corrosion protection properties of TiO_2 coatings by chromium doping. Corros Sci 68: 101-110.
10. Lei CX, Liu Y, Zhou H, Feng ZD, Du RG (2013) Photogenerated cathodic protection of stainless steel by liquid-phase-deposited sodium polyacrylate/TiO_2 hybrid films. Corros Sci 68: 214-222.
11. Doslu ST, Mert BD, Yazici B (2013) Polyindole top coat on TiO_2 sol-gel films for corrosion protection of steel. Corros Sci 66: 51-58.
12. Lai YK, Zhuang HF, Xie KP, Gong DG, Tang YX, et al. (2010) Fabrication of uniform Ag/TiO_2 nanotube array structures with enhanced photoelectron-chemical performance. New J Chem 34: 1335-1340.
13. Liu Y, Hu J, Li J (2011) Synthesis and photoactivity of the highly efficient Ag species/TiO_2 nanoflakes photocatalysts. J Alloys Compd 509: 5152-5158.
14. Li X, Xiong R, Wei G (2009) Preparation and photocatalytic activity of nanoglued Sn-doped TiO2. J Hazard Mater 164: 587-591.
15. Gao S, Li Z, Jiang K, Zeng H, Li L, et al. (2011) Biomolecule-assisted in situ

route toward 3D superhydrophilic Ag/CuO micro/nanostructures with excellent artificial sunlight self-cleaning performance. J Mater Chem 21: 7281-7288.

16. Jia F, Sun W, Zhang J, Li Y, Yang B (2012) A facile approach to fabricate three-dimensional ordered macroporous rutile titania at low calcination temperature. J Mater Chem 22: 2435-2441.
17. Cao Y, Yang W, Zhang W, Liu G, Yue P (2004) Improved photocatalytic activity of Sn4+ doped TiO2 nanoparticulate films prepared by plasma-enhanced chemical vapor deposition. New J Chem 28: 218-222.
18. Liu Y, Wang X, Yang F, Yang X (2008) Excellent antimicrobial properties of mesoporous anatase TiO2 and Ag/TiO_2 composite films. Microporous Mesoporous Mater 114: 431-439.
19. Wu M, Yang B, Lv Y, Fu Z, Xu J, et al. (2010) Efficient one-pot synthesis of Ag nanoparticles loaded on N-doped multiphase TiO_2 hollow nanorod arrays with enhanced photocatalytic activity. Appl Surf Sci 256: 7125-7130.
20. Zhao G, Cui X, Liu M, Li P, Zhang Y, et al. (2009) Electrochemical degradation of refractory pollutant using a novel microstructured TiO_2 nanotubes/ Sb-doped SnO_2 electrode. Environ Sci Technol 43: 1480-1486.
21. Cao Y, Zhang X, Yang W, Du H, Bai Y, et al. (2000) A bicomponent TiO_2/SnO_2 particulate film for photocatalysis. Chem Mater 12: 3445-3448.
22. Zhang FL, Zheng YH, Zhan YY, Lin XY, Zhang HH, et al. (2009) [Studies on Ag-TiO_2/KIT-6 composite nanosized photocatalyst]. Guang Pu Xue Yu Guang Pu Fen Xi 29: 2166-2170.
23. Wang Y, Yan Z, Wang X (2014) Photocatalytic degradation of Rhodamine B dye over novel porous TiO_2-SnO_2 nanocomposites prepared by hydrothermal method. Int J Photoenergy 3: 1-7.